

Influence of Clamping Conditions on Microstructure Compliance

Gerald Gerlach, Andreas Schroth and Patrick Pertsch

Dresden University of Technology, Institute of Precision Engineering,
01062 Dresden, Germany

(Received May 30, 1994; accepted February 21, 1995)

Key words: simulation, clamping, micromechanics

Many sensors and actuators, especially in the field of microsystem technology, use bending beams and plates which are fabricated monolithically by local thinning of a substrate (for instance, silicon). To describe the mechanical behavior of these elastic elements, the influence of clamping must often be considered because of its finite mechanical stiffness. Because the point of clamping under load shows rotational as well as translational deflection, elastic clamping can be principally modeled as spring elements. In this case the rotational clamping compliance is of outstanding importance. For most micromechanical clamping geometries, the values of the compliances of these spring element substitutes will be shown with their ranges of validity. Because the results of the investigations are presented parameterized, conclusions on the influence of the parameters of clamping can easily be drawn. This helps us to find the clamping geometry with the highest stiffness.

Symbols and Indices

A	area (of the cross section)
E	Young's modulus
E^*	effective Young's modulus
I	moment of inertia
M	torque
Q	transverse/ shear force
S	axial force
b	width of the structure
h	thickness of the structure

k	clamping coefficient
n	mechanical compliance
p	pressure
q	line pressure
x	horizontal coordinate direction
y	vertical coordinate direction
r	rotational value
x	horizontal value component
y	vertical value component
z	orthogonal value component
α	clamping geometry angle
β	shear angle
ε	strain
φ	rotation angle
κ	geometry constant
τ	shear stress
ν	Poisson's ratio
σ	stress
ξ	deflection

1. Introduction

The functional principle of most mechanical sensors is based on the bending of plates or beams as mechanical transducer elements.⁽¹⁾ The values of pressure, force or acceleration to be measured cause a deflection of the beam or plate and therefore, mechanical stresses and strains. These quantities are finally transformed into capacitive or piezoresistive changes which can be detected electronically.

To date, ideally rigid clamping conditions have generally been assumed in the analytical calculation of bending during the process of sensor design (Fig. 1(a)). This means that the cross-sectional areas at the clamping point can neither be translated nor rotated.

However, because of the elastic properties and the small size of miniaturized mechanical transducer elements compared to those of micromechanical sensors, the compliance of the clamping must be considered (Fig. 1(b)) in order to achieve exact results which are applicable to practical design purposes. Some important clamping geometries of micromechanical applications are shown in Fig. 2. They are mainly caused by the manufacturing microtechniques used (for instance, anisotropic etching, LIGA technology, surface micromachining, bonding and etch-back).⁽²⁻⁴⁾

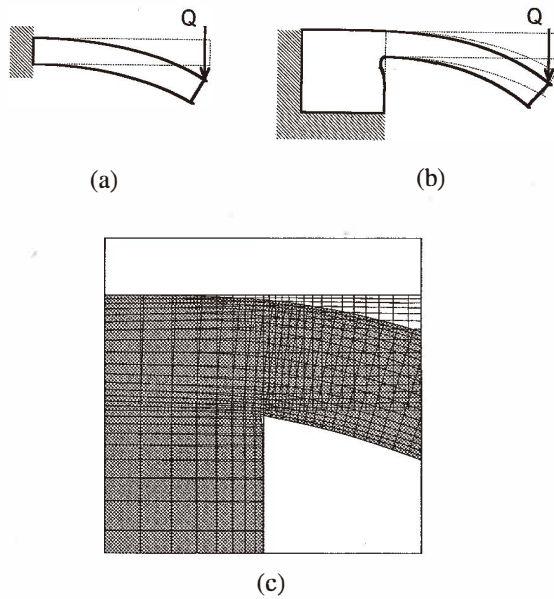


Fig. 1. One-side clamped bending beam with applied load. (a) Ideally rigidly clamped. (b) Real clamping. (c) Deformation in the clamping region.

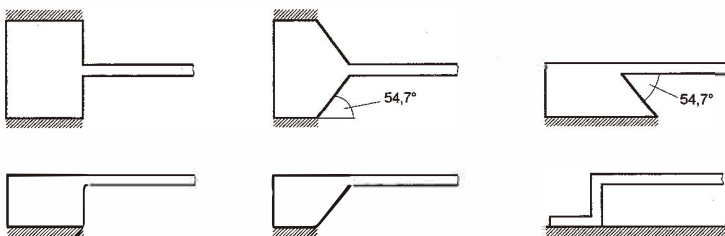


Fig. 2. Basic clamping geometries of micromechanical applications.

2. Model of Sensor Clamping

Figure 3 shows an example of a mechanical transducer element with typical clamping geometries and its deformation under an applied load. As can be seen from Fig. 1(c), not only the bending element but also the area of clamping will be deformed because of the limited stiffness of the clamping. Translational and rotational deflections of the clamping area can be characterized as shown in Fig. 3(a).

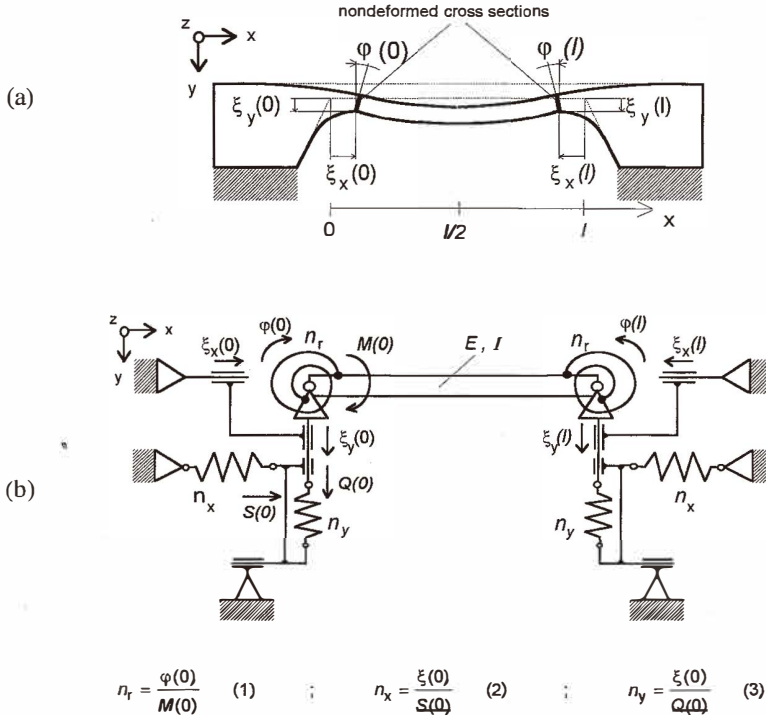
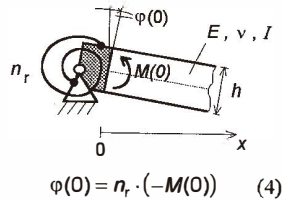


Fig. 3. Both-sides-clamped bending beam. (a) Deformed structure. (b) Modelling with concentrated network elements.

Assuming small beam deflections, the Bernoulli hypotheses of constantly flat beam cross-sectional areas can be assumed to be valid. Hence the position of the clamping cross-sectional area, which is the intersection of the clamping bulk and beam, can be described by means of two translational deflections, ξ_x and ξ_y , in the x - and y -directions, respectively, and one rotational motion characterized by an angle. Because the deformations are caused by the applied loads, the clamping region can be modeled by two translational compliances n_x and n_y and by one rotational compliance n_r , whereas beam and plate are considered to be transforming elements with ideal deformation behavior (Fig. 3(b)).⁽⁵⁾ Due to the restriction of small deflection both the translational and the rotational deformations can be superposed linearly.

Figure 4 shows the left part of the clamped bending beam of Fig. 3 with neglected translational deflections. For the rotational compliance n_r , the following can be assumed.

- Similar to the bending behavior of a beam or a plate, the deformation of the clamping region is determined by the moment of inertia I and Young's modulus E .



$$\varphi(0) = n_r \cdot (-M(0)) \quad (4)$$

Fig. 4. Torsional boundary condition at the left side of the beam.

- The compliance of the clamping region decreases as the thickness of the bending element is reduced.

Based on the above, the rotational compliance n_r can be described as follows:⁽⁶⁾

$$n_r = k_r \cdot \frac{h}{E^* \cdot I}. \quad (5)$$

The factor k_r describes the elastic influence of the transition region between clamping and the beam or plate and can be interpreted as a proportionality factor of the bending stiffness of a thick clamping bulk with a thin deformation (transducer) element.

Analogous to eq. (5) the translational compliances n_x and n_y can be written as

$$n_{x,y} = k_{x,y} \cdot \frac{1}{E^* \cdot b}. \quad (6)$$

Because the bending state is mostly used for micromechanical transducer elements, the rotational clamping compliance n_r must be taken into consideration for determining sensor behavior, whereas n_x and n_y in most cases of practical applications can be neglected. However, n_x in particular must be considered if membrane stresses appear, caused, for instance, by axially applied forces or large deflections (compare with section 6.2).

The values of the spring elements n_x , n_y and n_r (k_r and I) are determined by the concrete clamping geometry and the elastic properties (Young's modulus E , Poisson's ratio ν) of the material used.

3. Solution Strategy

Using the model shown in Fig. 3 the behavior of clamping of monolithic elements can be described by concentrated spring elements. Therefore the modeling of the influence of concrete clamping geometries is reduced to the determination of the spring coefficients k_r , k_x and k_y .

To solve this problem, the following procedures were used.

- i) Solution of linear (for determination of k_r) and nonlinear (to find $k_{x,y}$) differential equation of the elastic bending clamped beams to obtain an analytical equation for determination of the relevant spring coefficients k (section 4). The clamping springs will be taken into consideration as boundary conditions to solve the differential equations.
- ii) Modeling of important real clamping geometries, and simulation of load-dependent deflections of the entire structure by means of the finite-element-method (FEM) (section 5).
- iii) Calculation of the spring coefficients k from i) for parameter arrays of beam dimensions of real sensor geometries using calculated deflection values determined by FEM simulation in ii) (section 6).

Therefore, analytical solutions based on the classical theory of bending are used as reference solutions for the determination of spring properties according to eqs. (5) and (6).

Furthermore, the following assumptions are made.

- i) The stress-strain relation exhibits linear and isotropic material behavior.
- ii) The entire clamped beam or plate is considered to be monolithic and homogeneous. In reality, existing passivation, metallization, and other layers are neglected.
- iii) Beams or plates with thicknesses much smaller than their widths are mainly used. With $\varepsilon_z = 0$ a plane (one-dimensional) strain state is assumed, which leads to an effective Young's modulus of

$$E^* = \sigma_x / \varepsilon_x = \frac{E}{1 - \nu^2}. \quad (7)$$

- iv) The size of the clamping region is considered to be limited. Consequently, deflections of the chip edge areas away from the clamping regions can be neglected.

In the following, only beam geometries are discussed in order to determine the influence of clamping, because the clamping behavior of plates can primarily be reduced to beam clamping behavior.⁽⁷⁾

4. Theory of Beams and Plates

The reference solution for the determination of the influence of clamping is based on the calculation of the deformation of beams and plates by means of the linear theory of bending.⁽⁸⁾ This theoretical basis limits the range of validity to plates clamped on both sides with very small deflections compared to their thickness. In order to increase the validity range in the next step, membrane stresses must be taken into consideration, which cause additional axial forces in the x -direction.

4.1 Small deflections

4.1.1 Differential equation of bending beams

The bending state of a bending beam is determined by the torque M , the force Q and the pressure $q = p/b$ (b ... width of the beam) at the locations x and $x + dx$ of the ideal beam. The transverse forces Q must be taken into consideration, especially for short beams, because they cause shear deflection in addition to the bending state. The separation of bending from shear distortion is illustrated in Fig. 5.

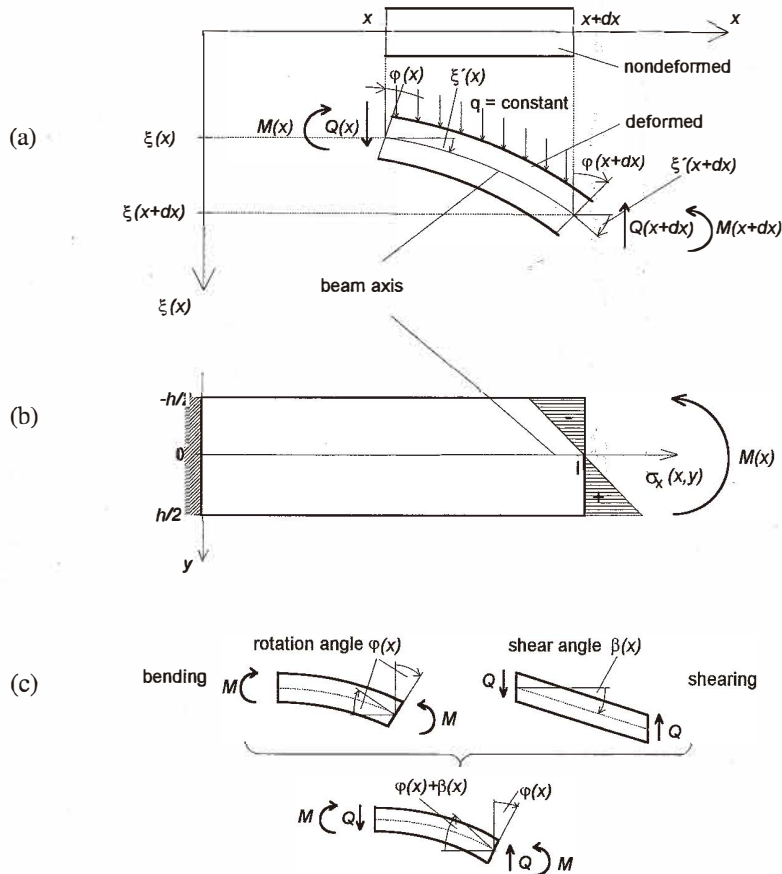


Fig. 5. Differential bending beam element ($\xi_y := \xi$; $\xi_x = 0$). (a) Determination of effective values. (b) Normal stress distribution σ_x . (c) Final deformation by superposition of bending and shearing.

From the well-known differential equation of bending,

$$E^* I \frac{d^4 \xi}{dx^4} = E^* / \xi'''' = q, \quad (8)$$

the following general solution for the deflection ξ in the y-direction can be derived:^(7,8)

$$\xi(x) = \xi_y(x) = \underbrace{\frac{1}{E^* I} \left\{ \frac{q}{24} x^4 + \frac{c_1}{6} x^3 + \frac{c_2}{2} x^2 + c_3 x + c_4 \right\}}_{\text{bending}} + \underbrace{\frac{\kappa}{G^* A_s} M(x)}_{\text{shear deflection}} \quad (9)$$

with

$$M(x) = - \left(\frac{q}{2} x^2 + c_1 x + c_2 \right) = - \frac{1}{E^* I} \frac{d^2 \xi}{dx^2}, \quad (10)$$

$$Q(x) = qx + c_1 = \frac{1}{E^* I} \frac{d^3 \xi}{dx^3}, \quad (11)$$

$$\kappa = \frac{A_s}{Q^2} \int_{A_s} \tau_{xy}^2 dA_s \quad (\kappa = 1.2 \text{ for rectangular cross sections}), \quad (12)$$

$$A_s = b \cdot h, \quad (13)$$

$$G^* = \frac{E^*}{2(1 + \nu)} \quad \text{and} \quad (14)$$

$$\beta(x) = - \frac{\kappa}{G^* A_s} Q(x). \quad (15)$$

For rectangular cross sections the normal stresses σ_x and the shear stresses τ_{xy} can be determined by means of eqs. (16) and (17).⁽⁷⁾

$$\sigma_x(x, y) = \frac{M(x)}{I} y \quad (16)$$

$$\tau_{xy}(x, y) = - \frac{3}{2} \frac{Q(x)}{bh} \left(1 - \frac{4y^2}{h^2} \right) \quad (17)$$

4.1.2 Clamping factor k_r

By solving the bending differential equation (8) for concrete load cases, the load-dependent deflection function $\xi(x, k_r)$ can be determined using eq. (4), with reference to the influence of clamping. Because the relationship between load and deflection is influenced by k_r , this clamping factor can be calculated backward from known deflection caused by known loads. This method of solution is shown in Table 1 for the example of a pressure plate clamped on both sides. The necessary calculations of the deflection behavior in the presence of a load can be performed by three-dimensional field calculation methods such as FEM.




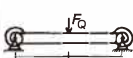

If the assumptions of Fig. 3 were valid, the value of k_r would also be equal for cases of different loads (Table 2).

Table 1

Bending coefficient k_r for both-sides-clamped plates with pressure load.

model:	
boundary conditions:	
(torque $M(x)$ continual in the plate) $q \neq 0$	
$\xi(0) = \frac{C_4}{E^* \cdot I} - \frac{x \cdot C_2}{G \cdot A_s} = 0$	(18)
$\xi(l) = \frac{q \cdot l^4}{24 \cdot E^* \cdot I} + \frac{C_1 \cdot l^3}{6 \cdot E^* \cdot I} + \frac{C_2 \cdot l^2}{2 \cdot E^* \cdot I} + \frac{C_3 \cdot l}{E^* \cdot I} + \frac{C_4}{E^* \cdot I} - \frac{x}{G \cdot A_s} \cdot \left(\frac{q \cdot l^2}{2} + C_1 \cdot l + C_2 \right) = 0$	(19)
$\xi'(0) = \varphi(0) + \beta(0) = -n_1 \cdot M(0) - \frac{x}{G \cdot A_s} \cdot Q(0) - \frac{k_r \cdot h \cdot C_2}{E^* \cdot I} - \frac{x \cdot C_1}{G \cdot A_s}$	(20)
$\xi'(l) = \varphi(l) + \beta(l) = n_2 \cdot M(l) - \frac{x}{G \cdot A_s} \cdot Q(l) - \frac{k_r \cdot h}{E^* \cdot I} \cdot \left(\frac{p \cdot l^2}{2} + C_1 \cdot l + C_2 \right) - \frac{x}{G \cdot A_s} \cdot (p \cdot l + C_1)$	(21)
solution of the integral values:	
$Q(x) = \frac{-q \cdot (l - 2 \cdot x)}{2}$	(22)
$M(x) = \frac{q \cdot (6 \cdot l^2 \cdot x - 6 \cdot l \cdot x^2 - l^3 + 12 \cdot h \cdot k_r \cdot (l \cdot x - x^2))}{12 \cdot (l + 2 \cdot h \cdot k_r)}$	(23)
$\xi'(x) = \frac{q \cdot (l - 2 \cdot x) \cdot ((l^2 \cdot x - l \cdot x^2 + h \cdot k_r \cdot (l^2 + 2 \cdot (l \cdot x - x^2))) \cdot G \cdot A_s + 6 \cdot x \cdot E^* \cdot I \cdot (l + 2 \cdot h \cdot k_r))}{12 \cdot E^* \cdot I \cdot G \cdot A_s \cdot (l + 2 \cdot h \cdot k_r)}$	(24)
$\xi(x) = \frac{q \cdot x \cdot (l - x) \cdot ((l^2 \cdot x - l \cdot x^2 + 2 \cdot h \cdot k_r \cdot (l^2 + l \cdot x - x^2)) \cdot G \cdot A_s + 12 \cdot x \cdot E^* \cdot I \cdot (l + 2 \cdot h \cdot k_r))}{24 \cdot E^* \cdot I \cdot G \cdot A_s \cdot (l + 2 \cdot h \cdot k_r)}$	(25)
determination of the bending coefficient k_r:	
$k_r = \frac{(384 \cdot \xi(l/2) \cdot l \cdot E^* \cdot I - q \cdot l^3) \cdot G \cdot A_s - 48 \cdot x \cdot E^* \cdot I \cdot q \cdot l^3}{2 \cdot ((-384 \cdot \xi(l/2) \cdot h \cdot E^* \cdot I) + 5 \cdot q \cdot h \cdot l^4) \cdot G \cdot A_s + 48 \cdot x \cdot E^* \cdot I \cdot q \cdot l^2}$	(26)

Table 2
Calculation of the bending coefficients k_r from displacements $\xi(x)$.

load	k_r	calc. from
	$\frac{\xi(l) \cdot E^* \cdot I}{l \cdot M_B \cdot h} - \frac{l}{2 \cdot h} \quad (27)$	$\xi(x=l)$
	$\frac{\xi(l) \cdot E^* \cdot I}{l^2 \cdot F_Q \cdot h} - \frac{l}{3 \cdot h} - \frac{\kappa \cdot E^* \cdot I}{G \cdot A_s \cdot h \cdot l} \quad (28)$	$\xi(x=l)$
	$\frac{2 \cdot \xi(l) \cdot E^* \cdot I}{l^3 \cdot q \cdot h} - \frac{l}{4 \cdot h} - \frac{\kappa \cdot E^* \cdot I}{G \cdot A_s \cdot h \cdot l} \quad (29)$	$\xi(x=l)$
	$\frac{l \cdot ((192 \cdot \xi(l/2) \cdot E^* \cdot I - F_Q \cdot l^3) \cdot G \cdot A_s - 48 \kappa E^* \cdot I \cdot F_Q \cdot l)}{8 \cdot h \cdot ((-48 \cdot \xi(l/2) \cdot E^* \cdot I + F_Q \cdot l^3) \cdot G \cdot A_s + 12 \kappa E^* \cdot I \cdot F_Q \cdot l)} \quad (30)$	$\xi(x=l/2)$
	$\frac{(384 \xi(l/2) \cdot l \cdot E^* \cdot I - q \cdot l^4) \cdot G \cdot A_s - 48 \kappa E^* \cdot I \cdot q \cdot l^3}{2 \cdot ((-384 \xi(l/2) \cdot l \cdot E^* \cdot I + 5 \cdot q \cdot l^4) \cdot G \cdot A_s + 48 \kappa E^* \cdot I \cdot q \cdot l^3)} \quad (31)$	$\xi(x=l/2)$

This conclusion is used to check the validity of the model in cases of different clamping geometries (one-sided and two-sided clamping) and loads (force, torque, pressure).

4.2 Large deflections

Distinct from the above-mentioned linear theory of bending, deflection-dependent membrane stresses must be taken into consideration if deflections ξ_y are of the same order of magnitude as the membrane or beam thickness itself. In particular, cases in which the applied load causes a lengthening of the neutral fiber in the middle plane, for instance, at bending plates or beams clamped on both sides, must be investigated.

The membrane stresses σ_{xm} only depend on the load to an even power because they are independent of the load direction and cannot become negative. These stresses cause an axial force S in the x -direction,

$$S = \sigma_{xm} \cdot hb, \quad (32)$$

which is followed by a deflection ξ_x of the clamping area as a result of the compliance of the clamping corresponding to eq. (2). Therefore the differential equation (8) must be modified so that we can consider S . It can be assumed that the membrane force S remains constant across the beam length. Then it can be concluded from eq. (2) that

$$n_x = \frac{\xi_x(0)}{S(0)} = \frac{\xi_x(0)}{S} \quad (33)$$

Because n_x should be independent of material and beam cross-section geometry, we can also assume the following, similar to the above-mentioned rotational clamping compliance:

$$n_x = k_x \frac{1}{E^* b}. \quad (34)$$

The calculation of k_x can be carried out analogously to the calculations in the case of small deflections. For this, values of deflections due to different loads will be calculated by means of finite-element analysis. The calculation procedure is demonstrated in Table 3 for a pressure-loaded plate clamped on both sides.

Thereby, the clamping coefficient k_x is determined using eqs. (46) – (49). Because k_x as well as k_r (compare eq. (40)) is unknown, two points of beam deflection must be used for the calculation of both coefficients. For further results, the deflections $\xi(l/2)$ and $\xi(l/4)$ will be used (compare section 6.2).

5. Finite-Element Model

For calculation of the characteristic clamping coefficients k_r and k_x with reference to eqs. (27) – (31) and (46), respectively, it is necessary to determine the deflection of clamped beams at certain locations, for instance, in the middle or at the end of the beam. Therefore clamped beams and plates are modeled by finite elements to simulate their behavior by means of a finite-element method program (ANSYS®⁽¹⁰⁾). Concerning the assumptions mentioned in section 3, square 8-node structural solid elements (STIF82) have been used to model the mechanical structure.

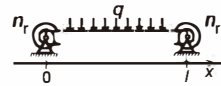
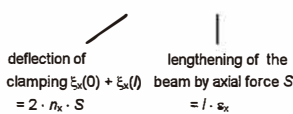
The different clamping shapes were simulated by the following model entities:

- i) The boundary of the clamping region in the model is formed by rigidly clamped edge nodes, which have a minimum distance to the end of the beam of twelve times the beam thickness h .
- ii) The clamping region contains from 50×50 to 100×100 finite elements.
- iii) The geometry of the beam is modeled by 16 layers of elements across the beam thickness.
- iv) By investigating the quality of the finite-element model, the expected linear relationships between both the reciprocal fineness of the net and the reciprocal size of the considered clamping region on the one hand, and simulation results (for instance, deflection) on the other hand, could be derived. Using this, the convergence value and the maximum deviations of k_r and k_x could be estimated.

6. Clamping Characteristics

As described above, the determination of rotational and translational clamping compliances was carried out by means of FEM simulations. In doing so the rotational clamping compliance n_r was calculated with small deflections, with reference to Table 2, as well as

Table 3
Determination of the coefficients k_r and k_x for pressure-loaded plates with large deflections.

	<p>model: $M(x) = \frac{q \cdot l}{2} \cdot x - \frac{q \cdot x^2}{2} - S \cdot \xi(x) + M(0)$ (35)</p>
boundary conditions:	$\xi(0) = 0$ (36)
	$\xi(l) = 0$ (37)
	$\xi'(0) = -n_r \cdot M(0)$ (38)
	$\xi'(l) = n_r \cdot M(l)$ (39)
displacement function⁽⁹⁾	
	$\xi(x) = \frac{q \cdot l^4}{16 \cdot u^4 \cdot E^* \cdot I} \cdot \frac{\tanh(u) - \gamma \cdot (\tanh(u) - u)}{\tanh(u)} \cdot \left(\frac{\cosh\left(u \cdot \left(1 - \frac{2 \cdot x}{l}\right)\right)}{\cosh(u)} - 1 \right) + \frac{q \cdot l^2}{8 \cdot u^2 \cdot E^* \cdot I} \cdot x \cdot (l - x)$ (40)
with	$\gamma = \frac{\tanh(u)}{2 \cdot k_r \cdot h \cdot u + \tanh(u)}$ (41)
and	$u^2 = \frac{S \cdot l^2}{4 \cdot E^* \cdot I}$ (42)
determination of the bending coefficient k_r from	
	$M(0) = -\gamma \cdot \frac{q \cdot l^2}{12} \cdot \frac{3 \cdot (u - \tanh(u))}{u^2 \cdot \tanh(u)}$ (43)
determination of the axial coefficient k_x from	
a) lengthening of the neutral fiber:	$\Delta l = \frac{1}{2} \cdot \int_0^l \left(\frac{d\xi}{dx} \right)^2 dx$ (44)
b) boundary condition of the elastic clamping:	$\Delta l = \frac{2 \cdot k_x \cdot S}{E^* \cdot b} + \frac{l \cdot S}{E^* \cdot h \cdot b}$ (45)
	 <p style="text-align: center;"> deflection of clamping $\xi_x(0) + \xi_x(l)$ lengthening of the beam by axial force S $= 2 \cdot n_x \cdot S$ $= l \cdot \epsilon_x$ </p>
c) equalization of eqs. (44) and (45) in consideration of eqs. (41) and (43):	
	$k_x = \frac{l}{2 \cdot h} \left(\frac{q^2 \cdot l^8}{E^* \cdot b^2 \cdot h^8} \cdot ((1 - \gamma) \cdot U_0 + \gamma \cdot U_1 - \gamma \cdot (1 - \gamma) \cdot U_2) - 1 \right)$ (46)
with	$U_0 = \frac{135 \tanh(u)}{16 u^9} + \frac{27 \tanh^2(u)}{16 u^8} - \frac{135}{16 \cdot u^8} + \frac{9}{8 \cdot u^6}$ (47)
	$U_1 = \frac{16 \cdot u^7 \cdot \tanh(u)}{27} - \frac{27}{16 \cdot u^6 \cdot \sinh^2(u)} + \frac{27}{4 \cdot u^8} + \frac{9}{8 \cdot u^6}$ (48)
	$U_2 = \frac{27}{16} \cdot \frac{(u - \tanh(u))^2}{u^9 \cdot \tanh^2(u)} \cdot (u \cdot \tanh^2(u) - u + \tanh(u))$ (49)

with large deflections, with reference to Table 3. The differences in the results for the clamping factor k_r were found to be marginal and are included in the deviations described below.

The influence of the translational clamping compliance n_x on the plate or beam deflection ξ_y can be neglected for small axial forces S . Because of this the determination of k_x using eq. (46) of Table 3 was carried out with nonlinear large deflection calculations including the already determined coefficient k_r .

Since for sensor applications the influence of n_r and n_x is revealed to be much greater than the influence of the translational clamping compliance n_y , this latter factor has not been determined.

6.1 Rotational clamping compliance n_r

Referring to eq. (5) the rotational clamping compliance is determined apart from elastic properties and beam thickness, only by the clamping coefficient k_r , which describes the clamping geometry. In the following, different influences of geometric properties and loads on k_r will be investigated.

6.1.1 Influence of beam geometry

As shown in Fig. 5, in addition to bending distortions of beams and plates, shear deformations also appear, which must be taken into consideration especially for very short beams ($l/h < 10$). Figure 6 shows an example of an ideal rigidly clamped beam ($n_x = 0$ and $k_x = 0$), which is affected by a shear force. If shear effects are neglected ($\kappa = 0$), an incorrect, merely virtual coefficient Δk_r will be obtained.

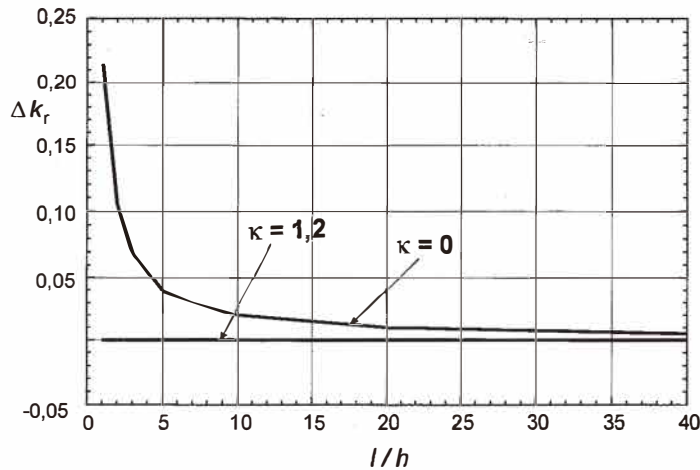


Fig. 6. Clamping coefficient Δk_r of an ideal rigidly clamped beam, with ($\kappa = 0$) and without ($\kappa = 1, 2$) taking shear forces into consideration.

6.1.2 Influence of load case

The dependence of the clamping coefficient k_r on the manner of loading of the bending beam was investigated. Table 4 shows the results of a common clamping geometry of an anisotropically etched (100) <110>-oriented silicon bar (clamping angle $\alpha = 54,74^\circ$).⁽²⁻⁴⁾ A maximum deviation of the k_r value from the mean of $\pm 2\%$ was observed.

6.1.3 Influence of clamping bulk geometry

The influence of different, and for practical applications, important, clamping shapes on the clamping coefficient k_r is summarized in Table 5. The deviations of the coefficient k_r reach only about 10 percent. The deviations are due to both dependences on the bending beam size for the mentioned length relations (Fig. 7) and dependences on the different loads.

Because Table 5 shows only some special clamping geometries, the transition from straight to sloped clamping and the transition from quarter-space to half-space clamping are shown in Figs. 8 and 9, respectively.

It can be seen that already at very small additional layer thicknesses h_k , the properties of the quarter-space clamping change to those of half-space clamping. On the other hand, the clamping angle α shows a comparatively small influence on k_r . Therefore it can be concluded that the clamping compliance is determined by a small region with the range of only 2–4 beam or plate thicknesses.

Table 4
Influence of load on the clamping coefficient k_r (maximum deviation $\Delta k_r/k_r = \pm 2\%$).


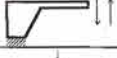
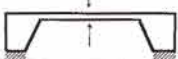

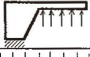
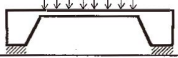
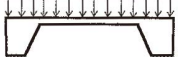


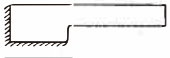

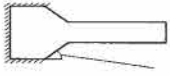
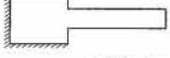
load	scheme	k_r
torque		0.7380
transverse force		0.7536
		0.7653
pressure		0.7644
		
		0.7791
		0.7807
		0.7800

Table 5
Geometry dependence of the clamping coefficient k_T .

clamping geometry	k_T
 sloped quarter-space clamping 54.7°	0.76 ± 0.08
 straight quarter-space clamping	0.65 ± 0.06
 sharp quarter-space clamping 54.7°	0.63 ± 0.06
 sloped half-space clamping 54.7°	0.44 ± 0.06
 straight half-space clamping	0.42 ± 0.04

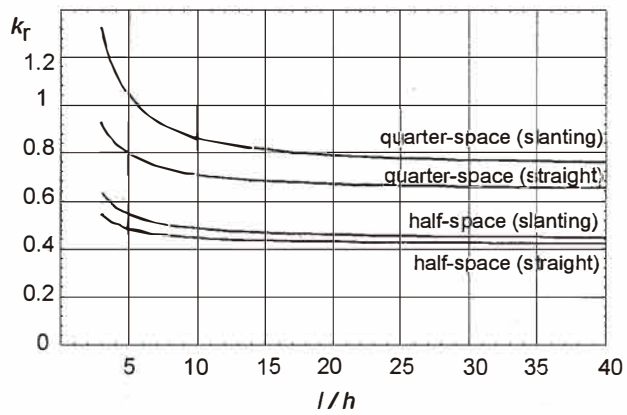


Fig. 7. Dependence of the clamping coefficient k_T on clamping geometry and beam length.

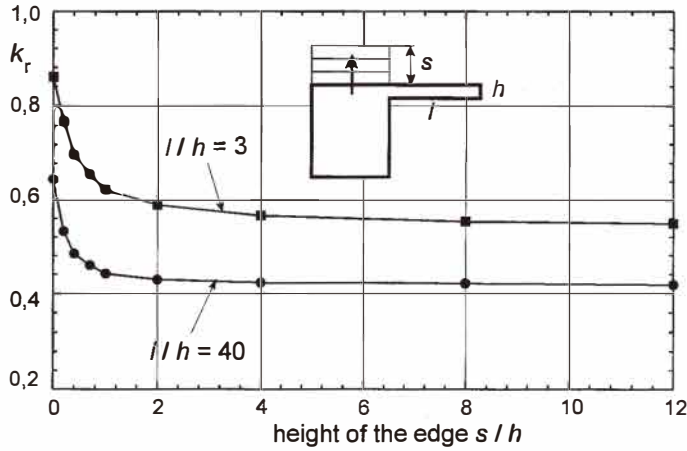


Fig. 8. Clamping coefficient k_r with transition from quarter-space to half-space clamping.

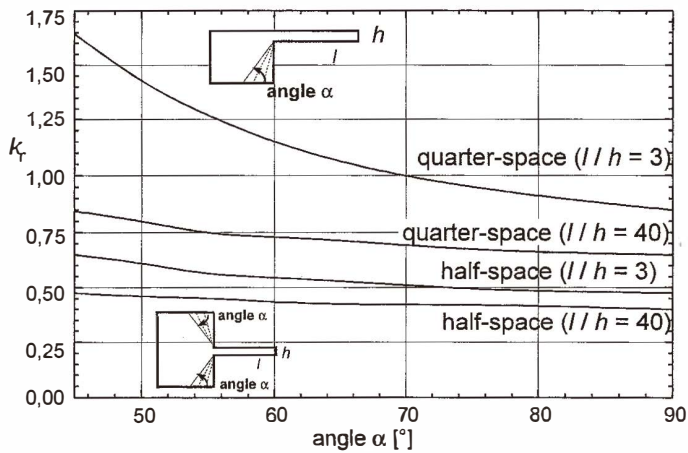


Fig. 9. Clamping coefficient k_r as a function of the clamping angle α .

6.1.4 Influence of large deflections

To investigate the influence of large deflections on the rotational clamping compliance n_r , the relationship between the clamping coefficient k_r , referring to Table 3, and the deflection of the beam was determined (Fig. 10(a)). This was carried out considering nonlinear geometric interrelations at large deflections using the FEM system.

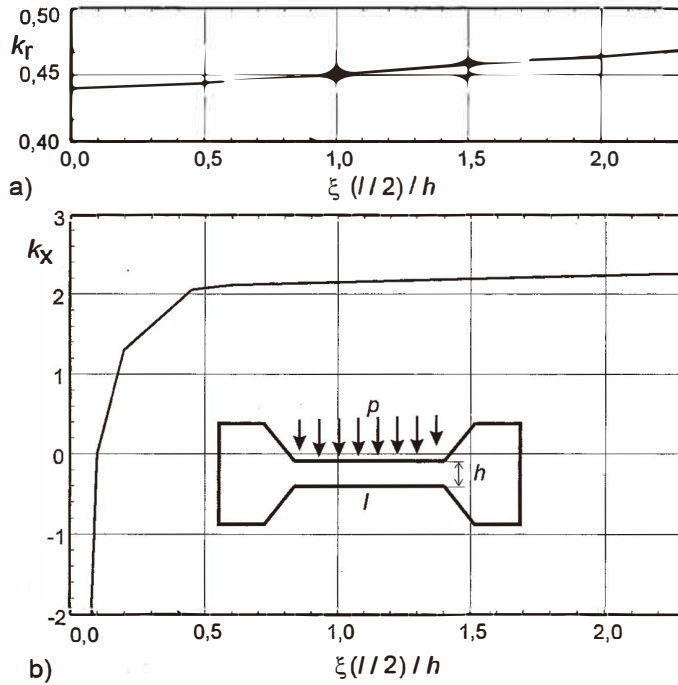


Fig. 10. a) Influence of large deflections on the clamping coefficient k_r .
 b) Influence of the beam deflection on the clamping coefficient k_x .

For pressure-loaded beams with clamping on both sides, the change of k_r in the range 0.44 to 0.46 can be neglected compared to the divergences induced by model errors and load case differences (see Table 5).

6.2 Translational compliance n_x

The translational compliance n_x of the clamping region is determined by the clamping coefficient k_x (cf. eq. (6)). This coefficient has been calculated considering large deflections, as shown in Table 3. The calculations have been carried out by means of analytical as well as FEM simulation programs. Deviations between the results of the two methods were less than 1% for all investigated cases. Hence it can be concluded that the analytical estimation of Table 3 reveals a high degree of validity.

6.2.1 Influence of beam deflection

Figure 10(b) shows the clamping coefficient k_x of the translational compliance n_x in the x -direction. For deflections $\xi = \xi_x$ larger than half the thickness of the plate or beam, k_x remains approximately constant. The small increase which can be seen in this range is

because eqs. (40)–(49) (Table 3) are valid only for deflections smaller than the thickness of the plate or beam. Smaller deflections ξ_y are followed by very small displacements ξ_x of the clamping area. Because of this, numerical errors of the simulation method used cause large divergences for the calculated values of k_x .

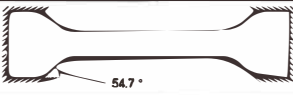
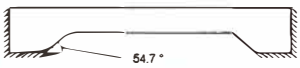
6.2.2 Influence of the geometry of the bulk

The influence of the shape of the clamping bulk on the translational compliance n_x is shown in Table 6 for the most important geometries. Deviations of k_x again are due to (similarly to k_r ; see Table 5) different loads, various beam sizes and the influence of deflection ξ_y , shown in Fig. 3. It is noteworthy that quarter-space clamping is six times more pliable than half-space clamping, instead of the expected factor of two.

6.3 Cross-sensitivity between n_r and n_x

An axial force in the x -direction applied to the half-space clamped structure causes displacements of the clamping region mainly in the x -direction (Fig. 11(a)). Distinct from this, an applied force at the structure with only quarter-space clamping causes additional

Table 6
Geometry dependence of the clamping coefficient k_x .

clamping geometry	k_x ($\xi/h \leq 2$)
	2.2 ± 0.5
	12.0 ± 4.0

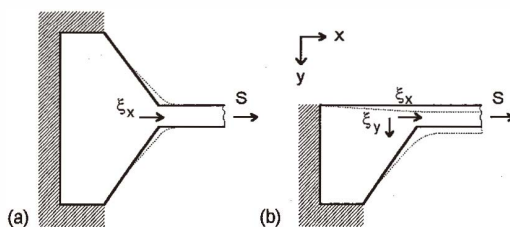


Fig. 11. Deformation of beam clamping with an axial force S . (a) Sloped half-space clamping. (b) Sloped quarter-space clamping.

deflections of the clamping cross section in the y -direction (Fig. 11(b)). This occurs because the axial force is exerted on the beam cross section at a point away from the neutral fiber of the beam, which causes an additional torque M . Because the analytical clamping model of the translational compliance n_x does not consider deflections in the y -direction, these displacements appear as a virtually increasing compliance n_r (Fig. 10(a)).

7. Conclusions

The presented investigations showed that clamping of real micromechanical bending beams and plates can be characterized by means of rotational and translational clamping compliances n_r and n_x . These compliances are influenced by clamping coefficients k_r and k_x , respectively, in addition to elastic material properties and geometrical properties of the clamped distorted body. For long beams (with length/thickness ratios ≥ 10) and even for the cases of most different loads these coefficients only depend on the concrete shape of the clamping geometry.

The calculation of the clamping coefficients is based on linear and nonlinear differential equations for bending beams. To solve these equations the clamping conditions are analytically modeled by rotational and translational clamping compliances. Using these models the coefficients could be calculated from known deflections of the beams and plates with the related known loads. The necessary relationships between deflections at different locations of the beam and various loads for different clamping shapes could be derived from the results of FEM simulation.

Investigations showed that the rotational clamping compliance n_r is of a comparatively high degree of importance because it affects the deformation behavior of the element already undergoing small deflections. The translational clamping compliance n_x in the axial direction must be taken into consideration only for double-sides-clamped beams or plates and in the case of large deflections in the vertical direction. Translational deflections of the clamping region in the y -direction, which could be modeled by a translational clamping compliance n_y , show, for most of the sensor applications, nearly no influence on their deformation behavior. Therefore they are neither investigated nor presented in this paper.

References

- 1 H.- J. Schorcht, M. Meissner and F. Wauro: Conference Proceedings of the 38th International Scientific Colloquium (Ilmenau, Germany, 1993) p. 462.
- 2 A. Heuberger, ed.: Mikromechanik (Springer-Verlag, Berlin, 1989).
- 3 S. Büttgenbach: Mikromechanik (B. G. Teubner, Stuttgart, 1991).
- 4 G. Gerlach: Mikromechanik, in Konstruktionselemente der Feinmechanik, ed. W. Krause (Carl Hanser Verlag, Munich and Vienna, 1993) 2nd ed., Chap. 14.
- 5 S. Hünemörder: Thesis, Dresden University of Technology, Institute of Technical Acoustics, Dresden (1981).
- 6 G. Gerlach, P. Pertsch and A. Schroth: Abstracts of Eurosensors VII, Budapest, (1993) p. 463.
- 7 P. Pertsch: Thesis, Dresden University of Technology, Institute of Technical Acoustics,

- Dresden (1993).
- 8 D. Rüdiger and A. Kneschke: *Technische Mechanik, Vol. 2 Festigkeitslehre* (B. G. Teubner, Leipzig, 1965).
 - 9 S. Timoshenko and S. Woinowsky-Krieger: *Theory of Plates and Shells* (McGraw-Hill, New York, 1959).
 - 10 ANSYS User's Manual for Revision 5.0, (Swanson Analysis Systems, Inc., Houston, 1992).
 - 11 P. C. Kohnke: *ANSYS User's Manual for Revision 5.0, Vol. IV Theory* (Swanson Analysis Systems, Inc., Houston, 1992).